Cu(In,Ga)Se2 absorber thinning and the homo-interface model: Influence of Mo back contact and 3-stage process on device characteristics

E. Leonard, L. Arzel, M. Tomassini, P. Zabierowski, D. Fuertes Marrón, and N. Barreau

Citation: Journal of Applied Physics **116**, 074512 (2014); doi: 10.1063/1.4891478
View online: http://dx.doi.org/10.1063/1.4891478
View Table of Contents: http://scitation.aip.org/content/aip/journal/jap/116/7?ver=pdfcov
Published by the AIP Publishing

$Cu(In,Ga)Se_2$ absorber thinning and the homo-interface model: Influence of Mo back contact and 3-stage process on device characteristics

E. Leonard,[1] L. Arzel,[1] M. Tomassini,[1] P. Zabierowski,[2] D. Fuertes Marrón,[3] and N. Barreau[1,a)]

[1]*Institut des Matériaux Jean Rouxel (IMN)-UMR 6502, Université de Nantes, CNRS, 2 rue de la Houssinière, BP 32229, 44322 Nantes Cedex 3, France*

[2]*Faculty of Physics, Warsaw University of Technology, Koszykowa 75, PL 00-662 Warsaw, Poland*

[3]*Instituto de Energía Solar–ETSIT, Technical University of Madrid, Ciudad Universitaria s.n., 28040 Madrid, Spain*

(Received 6 June 2014; accepted 16 July 2014; published online 20 August 2014)

Thinning the absorber layer is one of the possibilities envisaged to further decrease the production costs of $Cu(In,Ga)Se_2$ (CIGSe) thin films solar cell technology. In the present study, the electronic transport in submicron CIGSe-based devices has been investigated and compared to that of standard devices. It is observed that when the absorber is around 0.5 μm-thick, tunnelling enhanced interface recombination dominates, which harms cells energy conversion efficiency. It is also shown that by varying either the properties of the Mo back contact or the characteristics of 3-stage growth processing, one can shift the dominating recombination mechanism from interface to space charge region and thereby improve the cells efficiency. Discussions on these experimental facts led to the conclusions that 3-stage process implies the formation of a CIGSe/CIGSe homo-interface, whose location as well as properties rule the device operation; its influence is enhanced in submicron CIGSe based solar cells. © *2014 AIP Publishing LLC*. [http://dx.doi.org/10.1063/1.4891478]

I. INTRODUCTION

Solar cells based on $Cu(In,Ga)Se_2$ (CIGSe) thin-film technology have achieved energy conversion efficiency higher than 20% on both rigid and flexible substrates.[1–3] Such performance level is reached by stacks consisting of substrate/Mo/CIGSe/CdS/ZnO/ZnO:Al structures, in which the CIGSe layer is grown following vacuum based processes.[4] Although already industrially implemented,[5,6] this technology still needs to gain competitiveness in the market. With this goal, several issues should be addressed. One of them is the decrease of the thickness of CIGSe layer to reduce source material consumption and to increase processing speed without performance degradation.

Up to now, highest efficiencies are achieved by devices made of absorber layers whose thickness exceeds 2 μm.[1–4] Theoretical investigations suggest the CIGSe thickness could be reduced below 1 μm without major efficiency loss. Several groups have therefore investigated the behaviour of solar cells based on submicron CIGSe absorbers.[7–14] Rather similar conclusions are drawn from these investigations, observing two different regimes in photovoltaic parameters degradation: (i) the decrease of CIGSe thickness from 2 μm down to 1 μm hinders the short-circuit current (J_{sc}) because of lowered absorption probability of low energy photons; (ii) for absorbers with submicron thickness, additional open-circuit voltage (V_{oc}) and fill factor (FF) degradation are usually observed. Recent studies[8–14] assign the latter losses to increased carrier recombination probability at the Mo/CIGSe interface.

In the present work, solar cells with CIGSe thickness from 1.5 through 0.5 μm are studied. The determination of the mechanisms dominating carrier recombination suggests that the characteristics of the back contact and the absorber growth process parameters are key issues to minimize performance loss in submicron CIGSe-based solar cells.

II. EXPERIMENTAL DETAILS

A. Solar cells fabrication

The structure of the solar cells investigated in the present study consists of Mo/CIGSe/CdS/ZnO/ZnO:Al stacks. All these layers have been optimized for our laboratory's 2 μm-thick CIGSe baseline.

The substrates are 1 mm-thick soda-lime glass (SLG) microscope slides (1×3 in.^{2}); the Na_2O content is 14 wt. %. The back contact consists of 0.5 μm-thick DC-sputtered polycrystalline Mo layer which combines low sheet resistance and optimized permeability to Na-compounds of the substrate.

The CIGSe layer is grown in high vacuum by co-evaporation from elemental sources following the so-called 3-stage process.[4] The latter consists of first grow an $(In,Ga)_2Se_3$ layer (1st-stage, duration d_1), then supply exclusively Cu and Se until the Cu content of the growing film is over stoichiometry (2nd-stage, duration d_2), and finally supply In, Ga, and Se again until Cu content is under stoichiometry (3rd-stage, duration d_3). In order to minimize differences induced by the different film growth durations, the temperature of the substrates was kept constant at 580 °C during the whole deposition process (in contrast to conventional 3-stage process which implies two different substrate

a)Author to whom correspondence should be addressed. Electronic mail: nicolas.barreau@univ-nantes.fr.

TABLE I. Duration of each stage of the 3-stage process used to deposit absorbers with thicknesses from 1.5 μm to 0.5 μm.

Sample #	CIGSe_1.5	CIGSe_1.0	CIGSe_0.8	CIGSe_0.5
Stage 1 (d_1) (min)	35	25	18	12
Stage 2 (d_2) (min)	16	10	7	4.5
Stage 3 (d_3) (min)	3.5	2.5	1.8	1.2
$R_{3/1} = d_3/d_1$		1/10		
Thickness t_{CIGSe} (μm)	1.5	1.0	0.8	0.5

temperatures). All metal evaporation fluxes were similar from one run to the other. In order to vary the final thickness of the CIGSe, the durations of the three stages have been modified as detailed in Table I. One should notice that for all growths, the duration of stage 3 is one tenth of stage 1 (i.e., $R_{3/1} = 1/10$). The Cu-poor/Cu-rich/Cu-poor transitions have been followed in real time by the end-point detection method.[15]

The buffer layer consists of 50 nm-thick CdS deposited by chemical bath deposition (CBD) following our laboratory baseline recipe right after the absorbers are taken out of the deposition chamber. The window is made of ZnO(50 nm)/ZnO:Al(180 nm) layers, RF sputtered from ceramic targets. Finally, Ni/Al grids are deposited and 0.5 cm^2 cells mechanically scribed.

B. Thin film characterization

The CIGSe thin film composition has been determined by means of energy dispersive spectroscopy (EDS) using a JEOL-5800 scanning electron microscope (SEM) equipped with a germanium spectrometer PGT IMIX and operating at an accelerating voltage of 20 kV. The SEM observations were performed in a JEOL-7600 model microscope. The crystalline structure of the CIGSe films has been investigated by X-Ray diffraction (XRD) using a Brucker D8 system.

C. Solar cells characterization

The solar cell performance has been determined through standard $J(V)$ measurements performed at 25 °C under simulated AM1.5G illumination normalized to 100 mW/cm^2. External Quantum Efficiency (EQE) has been carried out at room temperature using a laboratory built system with a grating monochromator-based dual-beam setup under chopped light from a Xe lamp.

Temperature dependent $J(V)$ (i.e., $J(V,T)$) characteristics were measured in an evacuated Liquid Nitrogen (LN2)-cooled cryostat using a Keithley source measure unit Model 2601A. A window allows the illumination of the complete cell with a halogen lamp.

III. PRELIMINARY RESULTS

Representative $J(V)$ curves and EQE of devices with absorber thickness of 0.5 through 1.5 μm are plotted in Figs. 1(a) and 1(b), respectively. Fig. 1(a) shows that when the absorber thickness is less than 1 μm, not only the current density (J_{sc}) is affected as expected but also the open circuit voltage (V_{oc}) and the *FF* are severely impacted. Fig. 1(b) shows that the decrease of the absorber thickness leads to a loss in the EQE spectra for wavelengths above 550 nm; moreover, the absorption threshold assigned to absorber band gap (around 1100 nm) appears shifted towards shorter wavelengths when the CIGSe thickness is reduced. The present study aims at bringing elements for the better understanding of these observations.

The mean values of $x = [Ga]/([In] + [Ga])$ and $y = [Cu]/([In] + [Ga])$ are similar for all samples, namely, $x = 0.30$ (± 0.02) and $y = 0.90$ (± 0.02). SEM cross sections of the 1.5 μm and 0.5 μm thick CIGSe layers grown on the laboratory baseline SLG/Mo substrate are shown in Fig. 2. These images reveal that both layers have large grains, whose height is of the order of the layers thickness. The roughness of the films, investigated by atomic force microscopy, is around 40 nm (RMS) independently of the CIGSe film thickness. The XRD $\theta/2\theta$ patterns (not presented) show peaks revealing chalcopyrite single phase. The only changes that can be noticed from XRD are in the relative peak intensity (i.e., 112 versus 220/204) and peak broadening Γ. This information is summarized in Table II. All layers show I(112)/I(220/204) ratios close to 2.5, which points out randomly oriented CIGSe grains[16] independently of their thickness. The width of the 112 peak, referred to as $\Gamma(112)$, is the sum of three contributions, namely, the instrumental induced widening, the crystallite size contribution, and the spread of the lattice *d*-spacing. The broadening due to the measurement setup is identical for all samples since they were measured in the same conditions. As revealed by the SEM images shown in Fig. 2, the grains remain large, around 500 nm, even for the thinnest layer, ruling largely out a reduced crystallite size effect as the main origin of the changes in $\Gamma(112)$. Consequently, the broadening is most likely due to lattice

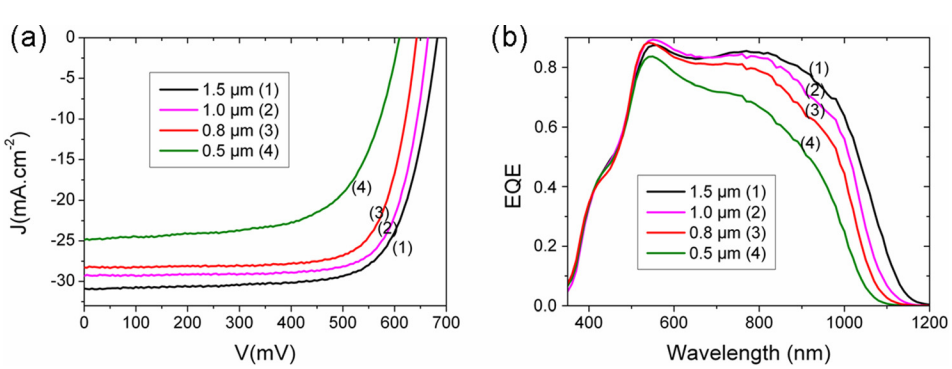

FIG. 1. (a) Illuminated current-voltage characteristics and (b) EQE of solar cells with absorber thicknesses from 1.5 μm to 0.5 μm.

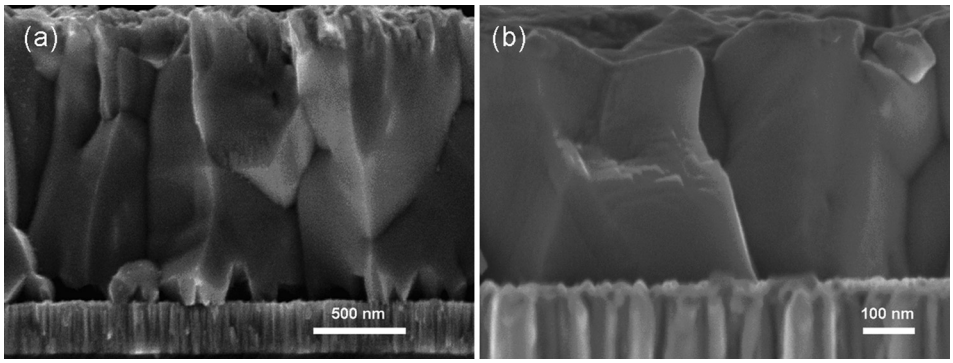

FIG. 2. SEM cross sections of the 1.5 μm-thick (left) and 0.5 μm-thick (right) CIGSe layers deposited following the 3-stage process on the standard SLG/Mo substrates.

distortion within the crystallites. Changes in $d(112)$ throughout the film depth could be the consequence of non uniform strain and/or non homogeneous chemical composition. Because these polycrystalline films are expected to be fully relaxed by the presence of extended defects (including dislocations, twins, and grain boundaries), lattice stress is most probably not at the origin of the changes in $\Gamma(112)$. The 3-stage process is known to induce V-shaped In/Ga gradients throughout CIGSe layers resulting from characteristic interdiffusion processes of cationic species induced by the compositional changes;[17] therefore, these gradients can be considered as the major reason for the broadening of the XRD peaks. Furthermore, as the peak becomes broader with increasing d spacing spreading, the In/Ga gradient is more pronounced in thicker films. As revealed by QE (Fig. 1), the absorption threshold of CIGS-layers shifts to higher energies as the layer thickness is reduced. This result indicates a variation of the bandgap minimum, and therefore of the corresponding In/Ga ratios, at a certain position within the layers, referred to as the Ga-notch: the thinner the layer, the more homogeneous the distribution of group III elements. The eventual implication of elemental distribution in V_{oc} and FF loss is much less straightforward than the observed blueshift in the absorption threshold. Consequently, the impact of absorber thinning on Mo/CIGSe films properties and the electrical characteristics of the resulting devices have been further investigated.

IV. ADVANCED ELECTRICAL CHARACTERIZATION

In order to further study the electronic losses mentioned in Sec. III, the changes in the transport mechanisms involved when the absorber thickness is decreased have been investigated with the help of temperature-dependent current-voltage measurements under AM1.5 illumination. Many articles review the quantitative analysis of such measurements; the extraction of parameter values and the use of temperature-dependent models allow to identify the physical location of dominant loss mechanisms in heterojunctions.[18–21] In the present study, all $J(V,T)$ characteristics could be successfully fitted using the single-diode model[22] described by

$$J(V) = J_{ph} - J_0\left\{\exp\left[\frac{e(V - R_sJ(V))}{Ak_BT}\right] - 1\right\} - \frac{(V - R_sJ(V))}{R_{sh}}. \quad (1)$$

The parameters thereby extracted are the saturation current J_0, the ideality factor A, the series resistance R_s, the shunt resistance R_{sh}, and the photocurrent J_{ph}.

The present analysis is based on the temperature dependence of the saturation current J_0, which can be described in the following equation:[18]

$$J_0 = J_{00}\exp\left(\frac{-E_a}{Ak_BT}\right), \quad (2)$$

where J_{00} is a pre-exponential factor only weakly T-dependent and E_a is the activation energy. The latter corresponds to the slope of the Arrhenius plot of $A\ln(J_0)$ presented in Fig. 3. As shown in Table III, the values of E_a so deduced decrease with decreasing absorber thickness. A similar evolution is observed when E_a is evaluated from the extrapolation to 0 K of the linear part of the temperature dependence of the cell V_{oc} (see Table III). This evolution indicates the changes in the dominating recombination mechanism when the absorber is thinned. For the 1.5 μm-thick CIGSe layer, E_a is similar to E_g, so the dominating recombination takes place

TABLE II. Broadening of CIGSe peak (112) and intensity ratio of CIGSe (112) and (220/204) peaks for absorber thicknesses from 1.5 μm to 0.5 μm.

	1.5 μm	1.0 μm	0.8 μm	0.5 μm
$\Gamma(112)$ (deg)	0.23	0.17	0.17	0.13
I(112)/I(220/204)	2.9	2.1	2.6	2.3

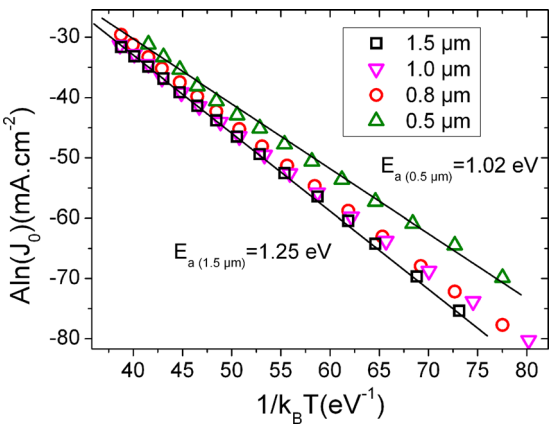

FIG. 3. Modified Arrhenius plot of corrected saturation currents as a function of the inverse temperature for solar cells with absorber thicknesses from 1.5 μm to 0.5 μm.

TABLE III. Activation energy E_a, E_{00} parameter, and diode parameters measured at room temperature for absorber thicknesses from 1.5 μm to 0.5 μm. The E_{00} parameter is determined from (Eq. (4)) for absorber thicknesses of 1.5 μm, 1.0 μm, and 0.8 μm and determined from (Eq. (3)) for the 0.5 μm thick absorber.

CIGSe thickness (μm)	E_a (eV) under illumination	E_a (eV) from Voc(T)	E_{00} (meV) under illumination	Ideality factor	J_0 (mA cm^2)	R_{sh} (Ω)	R_s (Ω)
1.5	1.25	1.20	13	1.53	1.8×10^{-9}	1.7×10^3	0.4
1.0	1.20	1.18	13	1.58	4.8×10^{-9}	2.4×10^3	0.5
0.8	1.15	1.16	12	1.70	5.7×10^{-9}	6.2×10^2	3.1
0.5	1.02	0.98	51	1.55	1.1×10^{-8}	2.2×10^2	2.0

in the space charge region (SCR). In contrast, for 0.5 μm thick CIGSe, E_a is lower than the E_g, suggesting interface recombination (IR) dominates the electronic transport. This change from SCR to IR could significantly decrease the cell efficiency when the absorber is thinned. Further information has been extracted from the investigation of the temperature dependence of A, as proposed in the literature. Indeed, Rau *et al.*[18–21] showed that such behaviour can provide information concerning the type and the location of the recombination process. Basically, two tunnelling process occurring in the CIGSe layer are possible, namely, tunnelling enhanced IR (i.e., TE-IR) and tunnelling enhanced SCR recombination (i.e., TE-SCR). In the case of TE-IR, the recombination process is described by a theory of thermo-ionic field emission[23] and the ideality factor is described as

$$A(T) = \frac{E_{00}}{k_B T} \coth\left(\frac{E_{00}}{k_B T}\right), \tag{3}$$

with $E_{00} = \frac{qh}{2}\sqrt{\frac{N_A}{m.\varepsilon_a}}$.

Here, E_{00} is the characteristic tunnelling energy, m is the carrier effective mass, N_A is the net acceptor concentration, and ε_a the semiconductor dielectric constant. As far as TE-SCR process is concerned, it can be described by recombination centres exponentially distributed in energy, leading to

$$\frac{1}{A} = \frac{1}{2}\left(1 - \frac{E_{00}^2}{3(k_B T)^2} + \frac{k_B T}{E^*}\right), \tag{4}$$

where $E^* = k_B T^*$ is the characteristic energy of the distribution of defects.[19]

Figure 4 shows the temperature dependence of inverse ideality factor for cells with different CIGSe thickness. The major impact of absorber thinning on $A^{-1}(T)$ plots is observed when the CIGSe is below 1.0 μm. Indeed, when the CIGSe layer thickness is between 1.5 μm and 1.0 μm, $A^{-1}(T)$ follows the model of TE-SCR. Low values of E_{00} ($\sim$15 meV, see Table III) are consistent with negligible tunnelling effect in good agreement with the literature.[18] In contrast, the $A^{-1}(T)$ plots of cells made from absorbers thinner than 1.0 μm cannot be adjusted by the TE-SCR model. Their linear shape rather implies dominating TE-IR; indeed, if $E_{00} \gg kT$, Eq. (4) reduces to $A^{-1} = kT/E_{00}$ and E_{00} can be extracted from the slope of the straight lines. All determined values of E_{00} are summarized in Table III; they significantly increase when the absorber is well below 1.0 μm. Several phenomena can induce such changes in E_{00}, namely, the effective doping density or the carrier effective mass (see expression of E_{00} in Eq. (4)). Regarding technological possibilities, the only reliable options to counteract this increased TE-IR contribution are either modify the sodium amount in the absorber, which is known to impact the effective doping N_A,[25,26] or modify the near-surface properties of the CIGSe layers. These issues are addressed in Sec. V.

V. INFLUENCE OF Mo CHARACTERISTICS AND CIGSe NEAR SURFACE PROPERTIES

In Sec. IV, it has been suggested that the performance drop observed when the absorber layer thickness is well below 1 μm could be due to TE-IR. Nevertheless, this conclusion does not inform on the location of the recombination. In order to provide the elements of answer, the present section aims at evaluating the influence of two parameters on the device performance, which are (i) the amount of sodium (Na) available during CIGSe growth and (ii) the absorber near-surface region properties.

(i) The amount of Na within CIGSe layer can be controlled through the tuning of Mo back contact properties; increasing the Mo layer density hinders its permeability to Na compounds.[27] 0.5 μm-thick CIGSe layers have been simultaneously deposited onto two different SLG/Mo substrates, namely, our laboratory standard SLG/Mo optimized for thick absorbers (the same as that used in Secs. I–IV, now referenced to as Mo^{ST}) and SLG/Mo stacks with much denser Mo layer (referenced to as Mo^{HD}). In the following, the

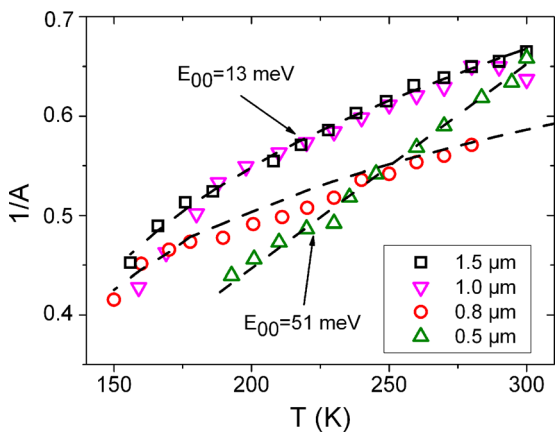

FIG. 4. Inverse of the ideality factor as a function of temperature for solar cells with absorber thicknesses from 1.5 μm to 0.5 μm. The characteristic tunnelling energy values E_{00} are calculated from ideality factor models.

TABLE IV. Overview of the best solar cell characterisation results and the diode parameters measured at room temperature for 0.5 μm thick CIGSe solar cell on Mo^{ST} with $R_{3/1} = d_3/d_1 = 1/10$, on Mo^{HD} with $R_{3/1} = 1/10$, and deposited on Mo^{ST} with $R_{3/1} = 2/9$.

	V_{oc} (mV)	J_{sc} (mA cm^{-2})	FF (%)	Eff. (%)	Ideality factor	J_0 (mA cm^{-2})	R_{sh} (Ω)	R_s (Ω)
$Mo^{ST}_{1/10}$: CIGSe reference on standard Mo	607	24.4	65.1	9.6	1.55	1.1×10^{-8}	2.2×10^{2}	2.0
$Mo^{HD}_{1/10}$: CIGSe reference on high density Mo	678	24.6	74.5	12.4	1.35	4.7×10^{-10}	1.3×10^{3}	0.9
$Mo^{ST}_{2/9}$: CIGSe modified recipe on standard Mo	673	24.3	72.5	11.9	1.45	2.1×10^{-10}	6.7×10^{3}	0.8

cells prepared from these structures are labelled as $Mo^{ST}_{1/10}$ and $Mo^{HD}_{1/10}$. One should notice that this approach is purely qualitative; it does not allow a quantitative evaluation of the changes in Na availability. Accordingly, one can only state higher Na availability on Mo^{ST} than on Mo^{HD}.

(ii) As detailed in Table I, the absorbers investigated in Secs. III and IV were grown by a derived isothermal 3-stage process, for which the duration of the 3rd stage is one tenth of the 1st stage ($R_{3/1} = 1/10$). Since the duration of the last stage (d_3) is likely to influence the absorber near-surface properties, its duration has been modified in a new batch of growth runs. The latter change also implied to modify the duration of the 1st stage (d_1) in order to keep 0.5 μm-thick layer and similar nominal Cu content (i.e., $y = 0.9$). In the following, the device referenced to as $Mo^{ST}_{2/9}$ has been fabricated with an overall 0.5 μm-thick absorber deposited on Mo^{ST} in conditions yielding $R_{3/1} = d_3/d_1 \sim 2/9$.

Table IV shows the photovoltaic parameters of the best cells of $Mo^{ST}_{1/10}$, $Mo^{HD}_{1/10}$, and $Mo^{ST}_{2/9}$. These results indicate that both the Mo-density (expected to change exclusively the Na availability) and the relative durations of 1st and 3rd stages ($R_{3/1}$) strongly impact the cell performance. Decreasing Na availability as well as increasing $R_{3/1}$yield better V_{oc} and FF, whereas J_{sc} remains unchanged. The origin of V_{oc} and FF improvement has been investigated through $J(V,T)$ measurements under illumination. Fig. 5(a) shows that the improvement can be linked to increase the activation energy E_a in $Mo^{HD}_{1/10}$ and $Mo^{ST}_{2/9}$ compared with $Mo^{ST}_{1/10}$. The inverse ideality factor model furthermore suggests that the TE-IR is not relevant to describe the dominant recombination process in $Mo^{HD}_{1/10}$ and $Mo^{ST}_{2/9}$. Indeed, Fig. 5(b) shows that $A^{-1}(T)$ follows a straight line above 0.5, which fits in the TE-SCR model with E_{00} tending to 0. In this case, the temperature dependence of inverse ideality factor is similar to that of classic Schockley-Read-Hall (SRH) recombination[24]

$$\frac{1}{A} = \frac{1}{2}\left(1 + \frac{k_B T}{E^*}\right). \tag{5}$$

These results show that the dominating recombination mechanism in 0.5 μm-thick CIGSe cells can be changed from TE-IR to TE-SCR by either increasing the density of the Mo-back contact (lower permeability to Na) or increasing $R_{3/1}$. In both cases, the tunnelling energy is significantly decreased, which reduces interface recombination and thereby yields better V_{oc} and FF.

VI. DISCUSSION

The results presented in Secs. I–V emphasize that decreasing the thickness of CIGSe grown following the 3-stage process from 1.5 to 0.5 μm impacts the optoelectronic behaviour of resulting cells. Moreover, in the case of 0.5 μm-thick absorbers, the optoelectronic characteristics of the devices depend on the availability of Na during the CIGSe growth as well as on the relative durations of the deposition stages. In the present section, all these results will be brought together in order to draw a clearer picture of the influence on the absorber thinning.

It has been observed that decreasing the absorber thickness below 1 μm in standard processing conditions yields decreased activation energy of saturation currents below the band gap, a fact not observed in thicker cells. Such a reduction of the activation energy denotes interface recombination mechanism as dominant. The first pending question is whether such interface recombination could be favoured by the macroscopic changes in material properties (i.e., In/Ga distribution) observed in Sec. III. The change in dominant recombination mechanism induced by slight process and back-contact properties modifications observed on

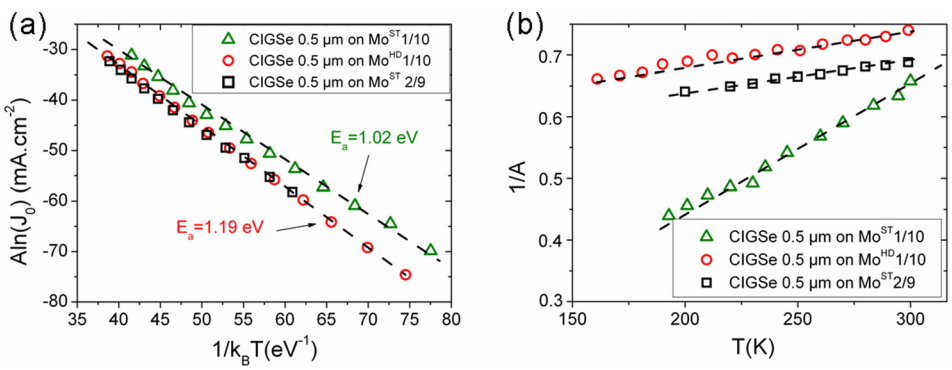

FIG. 5. (a) Modified Arrhenius plots of corrected saturation currents as a function of the inverse temperature and (b) inverse of the ideality factor A as a function of temperature for 0.5 cm^2 CIGSe solar cells deposited on Mo^{ST} with $R_{3/1} = d_3/d_1 = 1/10$, on Mo^{HD} with $R_{3/1} = 1/10$, and deposited on Mo^{ST} with $R_{3/1} = 2/9$.

0.5 μm-thick absorbers (see Sec. V) makes this hypothesis poorly probable.

The CIGSe device structure contains both hetero-interfaces (e.g., Mo/CIGSe and CIGSe/CdS) and homo-interfaces (e.g., grain boundaries and extended defects) where recombination is favoured. A major impact of thickness reduction is the location of the different interfaces relative to the junction field. The issue is then the determination of the interface dominating the electronic transport when the absorber thickness is decreased. As already proposed in the literature,[7–14] recombination at the Mo/CIGSe interface could become dominant. However, in this case, it would appear surprising that just a slight increase of $R_{3/1}$ ($Mo^{ST}{}_{1/10}$ vs. $Mo^{ST}{}_{2/9}$) could induce such drastic change in the dominant recombination path. Moreover, the investigation of the temperature dependence of the inverse ideality factor shows increased interface tunnelling with decreasing CIGSe thickness for the $Mo^{ST}{}_{1/10}$ series. Tunnelling is known favoured by a high acceptor density N_A or by a high density of traps in the junction field.[20] Therefore, if recombination at the back contact would dominate, its impact should be less pronounced with an increased N_A and thus a larger tunneling contribution in the near-surface region closer to the absorber/CdS junction; this is in contradiction to the present results if one assumes higher doping with increased Na availability. One can thus suggest that the recombination process is dominated rather by interfaces located in the space charge region than at Mo/CIGSe.

The present experiments show that for 0.5 μm-thick absorber, both the availability of Na during the CIGSe deposition and the value of $R_{3/1}$ impact the level of interface tunnelling. The location and/or the nature of the interface involved in the tunnelling therefore depends on (i) the thickness of the absorber, (ii) the amount of Na, and (iii) the value of $R_{3/1}$. The explanation we propose to link these 3 parameters to the tunnelling is based on basic correlations between the 3-stage process and the resulting CIGSe properties.

CIGSe layers grown by sequential 3-stage process can be considered as a stack of two layers labelled as CIGSe_1 and CIGSe_2. CIGSe_1, in contact with the Mo, results from the reaction of the $(In,Ga)_2Se_3$ layer formed during the 1st stage with Cu and Se supplied during the 2nd stage. This layer undergoes recrystallization when its nominal composition turns Cu-rich (i.e., $y > 1$),[28] which is concomitant with the beginning of Cu_2Se secondary phase segregation at the surface of the grains. CIGSe_2, which covers the CIGSe_1, is formed from the reaction of Cu_2Se with group III elements supplied during the 3rd stage.

The structural properties of the CIGSe_1/CIGSe_2 homo-interface and consequently the resulting density of crystalline defects at such homo-interface are likely to depend on:

(i) In/Ga gradients, because the location of the homo-interface coincides with the Ga notch.[17]
(ii) Na availability, since it has been shown that Na atoms are moved out of the grains when the layer is Cu-rich;[29] these Na atoms segregate to CIGSe_1 grains surface, in particular, to the CIGSe_1/Cu_2Se interface. The latter, parallel to the substrate, results in the CIGSe_1/CIGSe_2 homo-interface of completed layers after the third stage.

The location of the CIGSe_1/CIGSe_2 homo-interface relative to the CIGSe surface directly depends on $R_{3/1}$. Indeed, assuming similar CIGSe nominal composition (i.e., similar x and y), the location of the interface only depends on the thickness of CIGSe_1 (controlled by the duration of 1st stage) and the thickness of CIGSe_2 (controlled by the duration of 3rd stage). Therefore, the higher $R_{3/1}$, the further is the homo-interface from the CIGSe surface. For instance (see Fig. 6), if one considers CIGSe layers grown such that $R_{3/1} = 1/10$, in a first approach, the distance between the homo-interface and the CIGSe top surface (calculated from $t_{CIGSe} \times R_{3/1}$) is shifted from around 135 nm to around 45 nm, when the absorber thickness is reduced from 1.5 to 0.5 μm. For 0.5 μm absorber grown with $R_{3/1} = 2/9$, the homo-interface is located around 90 nm far from the surface, which corresponds to the distance in the case of 1 μm-thick CIGSe with $R_{3/1} = 1/10$.

To summarize, our model has identified the CIGSe homo-interface resulting from the recrystallization front taking place during the second and third stages of the growth process as the critical location where dominant recombination mechanisms control its transport properties. The nature of CIGSe_1/CIGSe_2 interface depends on the amount of Na available during the growth, whereas its location is directly dependent on the relative duration of growth stages $R_{3/1}$. One should, nevertheless, notice that changes in $R_{3/1}$ are also likely to modify the x profiles[30] and particularly absorption thresholds; however, these effects can be assumed negligible in 0.5 μm-thick absorbers since the gradient is already weak for $R_{3/1} = 1/10$ (see Sec. III). The results presented in Sec. V emphasize that TE-IR no more dominates the transport when either the availability of Na is decreased (i.e., $Mo^{HD}{}_{1/10}$ vs. $Mo^{ST}{}_{1/10}$) or when the $R_{3/1}$ is increased ($Mo^{ST}{}_{2/9}$ vs. $Mo^{ST}{}_{1/10}$) because

(i) decreasing the availability of Na during the growth is likely to decrease the density of defects and/or effective doping densities at the homo-interface, thus minimizing the probability of tunnelling,

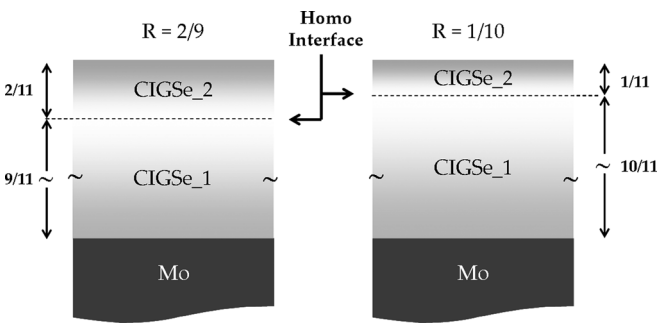

FIG. 6. Schematic representation of the homo-interface between CIGSe_1 and CIGSe_2 for two different absorbers deposited on Mo^{ST} with $R_{3/1} = d_3/d_1 = 1/10$ and $R_{3/1} = 2/9$. The location of the CIGSe_1/CIGSe_2 homo-interface relative to the CIGSe surface depends on the CIGSe thickness and the $R_{3/1}$ parameter.

(ii) moving the homo-interface away from the CIGSe/CdS electronic junction, where the electric field is the highest, is also expected to reduce tunnelling contributions.

VII. CONCLUSIONS

The influence of CIGSe thinning on solar cells performance was investigated. The results show that decreasing the absorber thickness below 1 μm enhances tunnelling interface recombination, which harms device efficiency. However, this detrimental effect is compensated either by decreasing the permeability of Mo back contact to sodium compounds or by proper modification of relative duration of growth stages. In order to explain these experimental facts, we propose a model which relies on the specific structure of CIGSe layers co-evaporated following the 3-stage process. We propose that this sequential growth process results in the formation of a CIGSe_1/CIGSe_2 homo-interface parallel to the substrate, whose defect distribution and location relative to the junction rule the submicron absorber based device operation. These results are expected to apply also to thicker CIGSe absorber layers and therefore to contribute to the understanding and optimization of 3-stage growth processing.

[1]P. Jackson, D. Hariskos, R. Wuerz, W. Wischmann, and M. Powalla, Phys. Status Solidi RRL **8**, 219 (2014).
[2]P. Jackson, D. Hariskos, E. Lotter, S. Paetel, R. Wuerz, R. Menner, W. Wischmann, and M. Powalla, Prog. Photovoltaics **19**, 894 (2011).
[3]A. Chirila *et al.*, Nat. Mater. **10**, 857 (2011).
[4]I. Repins, M. A. Contreras, B. Egaas, C. DeHart, J. Scharf, C. L. Perkins, B. To, and R. Noufi, Prog. Photovoltaics **16**, 235 (2008).
[5]E. Wallin, U. Malm, T. Jarmar, O. Lundberg, M. Edoff, and L. Stolt, Prog. Photovoltaics **20**, 851 (2012).
[6]K. Kushiya, Sol. Energy Mater. Sol. Cells **122**, 309 (2014).
[7]W. N. Shafarman, R. W. Birkmire, S. Marsillac, M. Marudachalam, N. Orbey, and T. Russell, in *Proceedings of the 26th IEEE Photovoltaic Specialist Conference*, Piscataway (1997), p. 331.
[8]T. Negami, S. Nishiwaki, S. Hashimoto, N. Kohara, and T. Wada, in *Proceedings of the 2nd World Conference on Photovoltaic Energy Conversion*, Vienna (1998), p. 1181.
[9]T. Dullweber, O. Lundberg, J. Malmström, M. Bodegard, L. Stolt, U. Rau, H. W. Schock, and J. H. Werner, Thin Solid Films **387**, 11 (2001).
[10]O. Lundberg, M. Bodegard, J. Malmström, and L. Stolt, Prog. Photovoltaics **11**, 77 (2003).
[11]M. Gloeckler and J. R. Sites, J. Appl. Phys. **98**, 103703 (2005).
[12]A. Kanevce, Ph.D. thesis, Colorado State University, 2007.
[13]Z. Jehl, Ph.D. thesis, Université Paris Sud-Orsay, 2012.
[14]A. Han, Y. Zhang, W. Song, B. Li, and W. Liu, Semicond. Sci. Technol. **27**, 035022 (2012).
[15]N. Kohara, T. Negami, M. Nishitani, and T. Wada, Jpn. J. Appl. Phys., Part 1 **34**, L1141 (1995).
[16]International Center for Diffraction Data, file 35–1102.
[17]A. M. Gabor, J. R. Tuttle, M. H. Bode, A. Franz, A. L. Tennant, M. A. Contreras, R. Noufi, D. G. Jensen, and A. M. Hermann, Sol. Energy Mater. Sol. Cells **41–42**, 247 (1996).
[18]V. Nadenau, U. Rau, A. Jasenek, and H. W. Schock, J. Appl. Phys. **87**, 584 (2000).
[19]U. Rau and H. W. Schock, Appl. Phys. A: Mater. Sci. Process. **69**, 131 (1999).
[20]U. Rau, Appl. Phys. Lett. **74**, 111 (1999).
[21]U. Rau, A. Jasenek, H. W. Schock, F. Engelhardt, and T. Meyer, Thin Solid Films **361–362**, 298 (2000).
[22]M. A. Green, *Solar Cells, Operating Principles, Technology and System Applications* (Prentice-Hall, 1982).
[23]F. A. Padovani and R. Stratton, Solid-State Electron. **9**, 695 (1966).
[24]T. Walter, R. Herberholz, and H. W. Schock, Solid State Phenom. **51**, 309–315 (1996).
[25]L. Stolt, J. Hedström, J. Kessler, M. Ruckh, K.-O. Velthaus, and H.-W. Schock, Appl. Phys. Lett. **62**, 597 (1993).
[26]D. J. Schroeder and A. A. Rockett, J. Appl. Phys. **82**, 4982 (1997).
[27]P. Bommersbach, L. Arzel, M. Tomassini, E. Gautron, C. Leyder, M. Urien, D. Dupuy, and N. Barreau, Prog. Photovoltaics **21**, 332 (2013).
[28]N. Barreau, T. Painchaud, F. Couzinié-Devy, L. Arzel, and J. Kessler, Acta Mater. **58**, 5572–5577 (2010).
[29]F. Couzinie-Devy, E. Cadel, N. Barreau, L. Arzel, and P. Pareige, Appl. Phys. Lett. **99**, 232108 (2011).
[30]M. Pawłowski, P. Zabierowski, R. Bacewicz, and N. Barreau, Thin Solid Films **535**, 336 (2013).